Article ID: 1006-8775(2016) S1-0057-10

CHARACTERISTICS OF THE LATENT HEAT DUE TO DIFFERENT CLOUD MICROPHYSICAL PROCESSES AND THEIR INFLUENCE ON AN AUTUMN HEAVY RAIN EVENT OVER HAINAN ISLAND

LI Jiang-nan (李江南)[1], MAI Xue-hu (麦雪湖)[1,2], LI Fang-zhou (李芳洲)[1], MAO Jiang-yu (毛江玉)[3]

(1. School of Atmospheric Sciences, Sun Yat-sen University, Guangzhou 510275 China; 2. Foshan Meteorological Service, Foshan, Guangdong 528000 China; 3. LASG, Institute of Atmosphere Physics, Chinese Academy of Science, Beijing 100029 China)

Abstract: We analyzed cloud microphysical processes' latent heat characteristics and their influence on an autumn heavy rain event over Hainan Island, China, using the mesoscale numerical model WRF and WRF-3DVAR system. We found that positive latent heat occurred far above the zero layer, while negative latent heat occurred mainly under the zero layer. There was substantially more positive latent heat than negative latent heat, and the condensation heating had the most important contribution to the latent heat increase. The processes of deposition, congelation, melting and evaporation were all characterized by weakening after their intensification; however, the variations in condensation and sublimation processes were relatively small. The main cloud microphysical processes for positive latent heat were condensation of water vapor into cloud water, the condensation of rain, and the deposition increase of cloud ice, snow and graupel. The main cloud microphysical processes for negative latent heat were the evaporation of rain, the melting and enhanced melting of graupel. The latent heat releases due to different cloud microphysical processes have a significant impact on the intensity of precipitation. Without the condensation and evaporation of rain, the total latent heating would decrease and the moisture variables and precipitation would reduce significantly. Without deposition and sublimation, the heating in high levels would decrease and the precipitation would reduce. Without congelation and melting, the latent heating would enhance in the low levels, and the precipitation would reduce.

Key words: heavy rain; numerical simulation; microphysical process; latent heat
CLC number: P426.6 **Document code:** A
doi: 10.16555/j.1006-8775.2016.S1.006

1 INTRODUCTION

Cloud microphysical processes are a critical scientific issue in regard to precipitation and clouds; however, research into these processes is limited because of the lack of observations. Today, research into the cloud-scale simulation (grid spacing less than 5 km) of heavy rain process using high resolution mesoscale modeling is increasing with the rapid development of computer technology. The simulation results from high resolution models are useful for the understanding of complicated cloud microphysical processes (e.g., Meng et al.[1-2]; Lin et al.[3-4]; Li et al.[5-6]). Therefore, research into the impact of the cloud microphysical processes on heavy rain is gradually increasing. For example, Wang et al.[7] simulated the cloud microphysical process of heavy rain in South China using the MM5 moist physical explicit scheme. Their results indicate that cold cloud with ice phase resulting from convection is the main cloud microphysical process during the heavy rain in the southern area. This implies that the warm cloud processes with water in the water phase rather than ice phase can only cause wide-range precipitation with low intensity.

Wang et al.[8] also investigated the supercooled water in convective clouds and determined that the cloud's vertical velocity and ice phase have a substantial impact on the supercooled water in the cloud. When the vertical velocity is large, the ice phase will occur and coagulate with supercooled water. With the evaporation, supercooled water will decrease rapidly, and precipitation will occur. Instead, with small vertical velocity and no ice phase particle,

Received 2015-06-17; **Revised** 2016-04-03; **Accepted** 2016-07-15
Foundation item: National Natural Science Foundation of China (41275060); National Key Basic Research Program of China (2014CB953903); National Natural Science Foundation of China (41275145); Fundamental Research Funds for the Central Universities (13lgjc03)
Biography: LI Jiang-nan, Ph.D., primarily undertaking research on numerical simulation and cloud physics.
Corresponding author: LI Jiang-nan, e-mail: essljn@mail.sysu.edu.cn

supercooled water will remain, and precipitation will not occur.

The research of Fovell and Ogura[9] indicated that the melting of graupel is the main source of the precipitation during the squall lines process over the mid-latitudes. Tao et al.[10] stated that the main cloud microphysical processes of convective cloud areas and stratiform cloud areas were significantly different. During the process of tropical squall lines, the main cloud microphysical processes in the convective cloud areas are condensation, cloud water collected by rainwater, and the melting of graupel. The main cloud microphysical processes over stratiform cloud areas are deposition, evaporation, melting, and collection of ice phase particles. Colle et al.[11] stated that condensation, deposition of snow, cloud water collected by rainwater, and melting of cloud water are important microphysical processes. This shows that there are substantial differences in the cloud microphysical processes of different climate systems. Therefore, further studies are needed to understand these processes in detail.

In recent years, heavy rain occurred frequently in Hainan Island, China, during autumn, which caused great damage to the region and considerable concern amongst local residents. However, studies of this event have mainly focused on the interaction between the circulation background and large-scale climate systems (e.g., Zhang[12]; Wu et al.[13]; Ma et al.[14]; Zhao et al.[15]). Furthermore, there is little research into cloud microphysical process of heavy rain.

In this study, we conducted several simulation experiments of the heavy rain event over Hainan Island that occurred in October 2010 using the mesoscale numerical model WRF and the WRF-3DVAR system. The research focused on the main cloud microphysical processes of the heavy rain event and the three-dimensional structure of its latent heat budget. We also analyze the impact of varying latent heat due to different cloud microphysical processes on the development of heavy rain.

2 OVERVIEW OF THE HEAVY RAIN EVENT

During the national day holidays in 2010, most areas of Hainan Province were affected by a storm flood disaster. This heavy rain event broke the record for October since 1961 for high continuous heavy rainfall, large area and persistence. The historical record for precipitation intensity was also broken in some areas. This heavy rain event can be divided into three phases. The first phase was from September 30 to October 2 in which heavy rain occurred in the middle–south region of Hainan. In the second phase, from October 3 to 5, the precipitation substantially increased. The whole of Hainan Island was affected by the rainstorm, except for Dongfang and Changjiang in the northwest area. The third phase began after October 5, in which the heaviest rain occurred; the precipitation registered in Qionghai from October 5 to 6 even reached 711.3 mm.

3 EXPERIMENTAL DESIGN AND VERIFICATION OF THE SIMULATION RESULTS

In this study, we simulated the heavy rain event during the period of heaviest rainfall, which was between 00 UTC on 5 October 2010 and 00 UTC on 6 October 2010 (universal time is used throughout this study). The experiments used the MERCATOR projection and triple nested grid. The grid intervals are 36, 12 and 4 km respectively. The top of the model is 50hPa, and 28σ layers of uneven depth were set vertically. The control experiment used global grid reanalysis FNL data from NCEP/NCAR with a 1° × 1° spatial resolution and 6 h temporal resolution. The initial conditions were adjusted by assimilating the radar radial velocity and reflectivity factor data with the WRF-3DVAR system. The physical parameterization schemes are listed in Table 1.

Table 1. The parameter setting of the physical processes in the simulation experiments.

Region	d01	d02	d03
Convective parameterization scheme	Grell-Devenyi ensemble scheme	Grell-Devenyi ensemble scheme	NONE
Cloud microphysical scheme	WDM6	WDM6	WDM6
Boundary layer scheme	YSU	YSU	YSU
Long wave radiative scheme	RRTM	RRTM	RRTM
Short wave radiative scheme	Dudhia	Dudhia	Dudhia

Figure 1 illustrates the observations of the largest precipitation center around Qionghai in the mid-east

area of Hainan. The highest rainfall observed was above 700 mm. The accumulated precipitation decreased from east to west. The intensity of the precipitation center from the simulation experiment was similar to the observations; in the experiments, the maximum center is also located around Qionghai in the mid-east area of Hainan. The distribution of precipitation is consistent with the observations and also decreases from east to west. Therefore, in general, the simulation of precipitation is relatively consistent with the observations.

The comparison presented in Fig. 2 was based on the observation data from the automatic station at Tanmen Middle School in Qionghai (19.2° N, 110.6° E). The comparison region is located within the area with accumulated precipitation above 700 mm in the simulation experiments (19.155–19.176° N, 110.32–110.39° E).

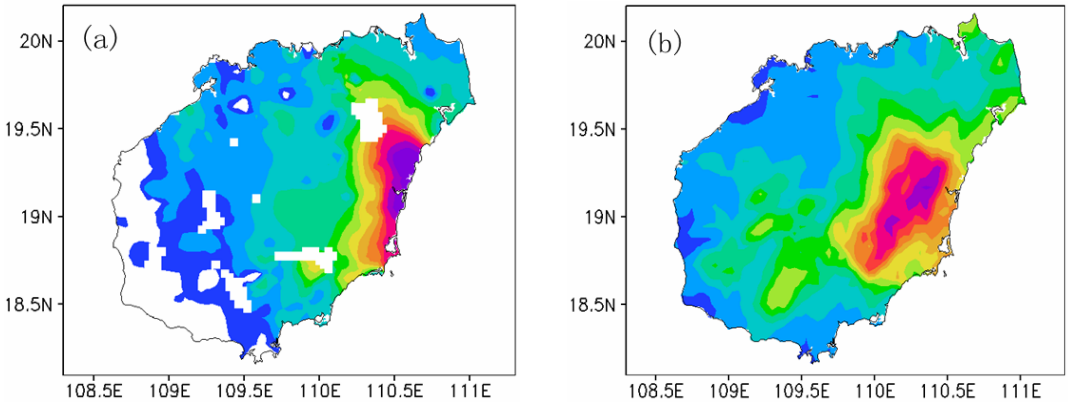

Figure 1. Accumulated precipitation of Hainan Island from 00 UTC 5 October 2010 to 00 UTC 6 October 2010 in region D03 (unit: mm). (a) Observation; (b) Simulation.

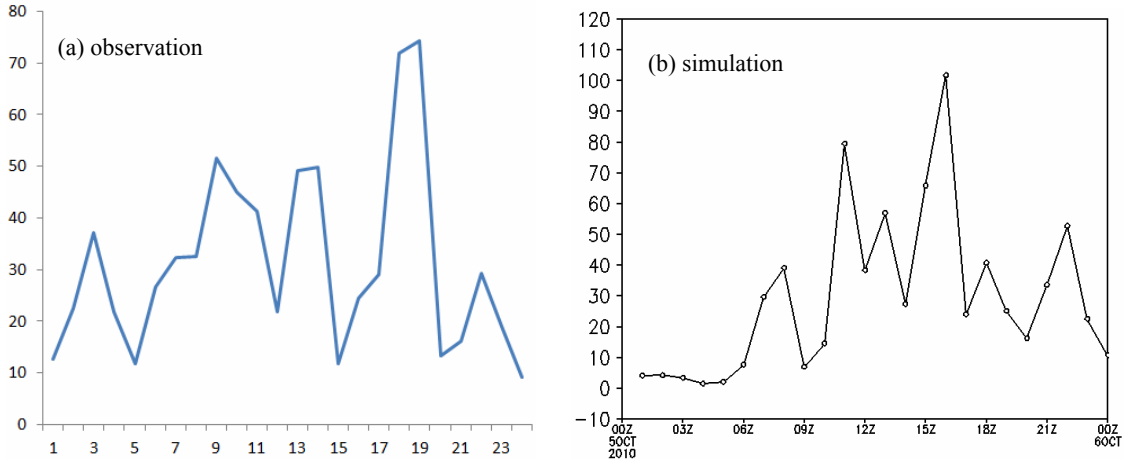

Figure 2. Hourly precipitation in the center of largest precipitation (unit: mm).

4 CHARACTERISTICS OF THE LATENT HEAT PROFILE

Figure 2 shows that there were several significant variations in the development processes of the precipitation intensity in the rainstorm center during the heavy rain event. Among these, the strongest development process commenced at 14 UTC, developed at 15 UTC, matured in 16 UTC and ended at 17 UTC. The maximum hourly precipitation exceeded 100 mm during the process. This experiment uses the WDM6 cloud microphysics scheme, which includes 6 hydrometeors (water vapor, cloud water, rainwater, cloud ice, snow, and graupel) and 38 cloud-microphysical transformation processes.

Cloud microphysical processes are accompanied by variations in the latent heat budget. To investigate these latent heat characteristics, six classes are stratified, namely, condensation (con), evaporation (rev), deposition (dep), sublimation (sub), freezing (frz), and melting (mlt). Processes without phase changes are neglected. The latent heating rates of the microphysical processes were calculated using the following equations.

$$Q_{\mathrm{con}} = L_v \times (P_{\mathrm{cond}} + P_{\mathrm{rcond}} + P_{\mathrm{cact}}) / C_{\mathrm{pm}} \quad (1)$$

$$Q_{\mathrm{evp}} = L_v \times \left(P_{\mathrm{cevp}} + P_{\mathrm{revp}} + P_{\mathrm{gevp}} + P_{\mathrm{sevp}}\right) \Big/ C_{\mathrm{pm}} \quad (2)$$

$$Q_{\mathrm{frz}} = L_f \times \left(P_{\mathrm{ihmf}} + P_{\mathrm{ihtf}} + P_{\mathrm{gfrz}} + P_{\mathrm{iacr}} + P_{\mathrm{gacr}} + P_{\mathrm{isacr}} + 2 \times P_{\mathrm{aacw}}\right) \Big/ C_{\mathrm{pm}} \quad (3)$$

$$Q_{\mathrm{mlt}} = L_f \times \left(P_{\mathrm{smlt}} + P_{\mathrm{imlt}} + P_{\mathrm{gmlt}} + P_{\mathrm{seml}} + P_{\mathrm{geml}}\right) \Big/ C_{\mathrm{pm}} \quad (4)$$

$$Q_{\mathrm{dep}} = L_s \times \left(P_{\mathrm{idep}} + P_{\mathrm{sdep}} + P_{\mathrm{gdep}} + P_{\mathrm{igen}}\right) / C_{\mathrm{pm}} \quad (5)$$

$$Q_{\mathrm{sub}} = L_s \times \left(P_{\mathrm{isub}} + P_{\mathrm{ssub}} + P_{\mathrm{gsub}}\right) / C_{\mathrm{pm}} \quad (6)$$

$$Q_{\mathrm{all}} = Q_{\mathrm{con}} + Q_{\mathrm{evp}} + Q_{\mathrm{frz}} + Q_{\mathrm{mlt}} + Q_{\mathrm{dep}} + Q_{\mathrm{sub}} \quad (7)$$

where P_{x} represents different conversion rates of cloud microphysical processes (unit: $\mathrm{kgkg^{-1}s^{-1}}$); L_{V}, L_{f}, L_{s} represent latent heat of phase changes per unit of mass during condensation, congelation and deposition processes, respectively (unit: $\mathrm{Jkg^{-1}}$);and C_{pm} represents the specific heat at constant pressure of the moist air (unit: $\mathrm{Jkg^{-1}K^{-1}}$). The total latent heating profile (Fig.3) shows that in the mature stage (15 UTC, 16 UTC), the largest heating center was above 8 km and the maximum reached 30 $\mathrm{Kh^{-1}}$. However, in the developing and decaying stages, the heating center was only 5 km high, which suggests that the heating in high levels was significantly weakened. The condensation contributed most out of the investigated sources of latent heat. In the formation and decay stages of the heavy rain, the heating due to condensation increased with height initially and then decreased to zero. In the developing and mature stages, two heating centers occurred vertically; one center was located above the melting layer and the other was beneath it. The condensation heating above the melting layer mainly resulted from the condensation of water vapor into cloud water, which is consistent with the analysis of moisture variables suggesting that plentiful supercooled water was present above the melting layer. The latent heating due to the deposition, congelation, melting and evaporation all strengthened initially and then weakened during the entirety of the heavy rain event. However, the variations of the latent heat due to condensation and sublimation were relatively small. The latent heat due to deposition and congelation contributed mainly to the heating of the levels above 6 km, whereas the latent heat due to melting and evaporation contributed to the cooling of low levels. The precipitation enhanced with the development of the rainstorm and the effect of the evaporation of cloud water and rainwater were substantially strengthened. The total latent heating at 16 UTC was negative under 2 km, after which the heavy rain event began to decay.

The negative latent heating was mainly distributed under 2 km (Fig. 4); however, the positive latent heating can reach above 12 km. Compared with the negative latent heating intensity, the positive latent heat intensity was significantly stronger. During the stages of development of the heavy rain, the positive latent heating center was 6-8 km higher than the melting layer. With the developing of the heavy rain, its maximum can exceed 40 $\mathrm{K\ h^{-1}}$. The negative latent heating center was around 4 km. Its intensity also slightly increased with the development of heavy rain. When the heavy rain started to decline and dissipate, the latent heating in high levels weakened significantly. The height of the heating center and the negative latent heating both gradually reduced under the melting layer.

5 CHARACTERISTICS OF THE LATENT HEAT BUDGETS

To further investigate the changes in the characteristics of the latent heat budget in response to the phase change in cloud microphysical conversions, we analyzed the latent heat release due to the phase change in cloud microphysical processes using the numerical model. The formulas are as follows:

$$\begin{aligned} Q &= \iiint L_x \times P_x(x,y,z) \times \rho(x,y,z) \times dxdydz \\ &= \sum_{i,j,k} L_x \times P_x(i,j,k) \times \rho(i,j,k) \times \Delta x \times \Delta y \times \Delta z(k) \end{aligned} \quad (8)$$

where Q represents the cloud microphysical latent heating rate; L_{x} is the latent heat amount due to the phase change; L_{v}, L_{f}, L_{s}, P_{x} are conversion rates of different cloud microphysical processes; ρ stands for air density; Δx, Δy are grid intervals in the x and y direction, respectively; and Δz is the spacing of the vertical model layers.

The vertical integral of the latent heat release due to phase change in cloud microphysical processes was calculated over three time periods: 1400–1500, 1500–1600, and 1600–1700 UTC, which represent the forming, developing, and decaying stages, respectively. The integral area is also 19.155–19.176°N, 110.32–110.39°E, selected from region D03. Table 2 illustrates the latent heat releases of all processes and their contribution percentages towards positive/negative latent heat. The condensation of water vapor into cloud water contributed the largest latent heat amount in different stages of the heavy rain event and its contribution was far greater than that of other microphysical processes. The main cloud microphysical processes of positive latent heat release are the condensation of water vapor into cloud water, the condensation of rainwater, and the deposition growth of cloud ice, snow and graupel. The main cloud microphysical processes of negative latent heat release are the evaporation of rainwater and the melting of graupel and its enhanced melting. During the two periods of the developing stage, 14–15 UTC and 15–16 UTC, there was little difference in the latent heat releases due to different microphysical processes. However, in the decaying stage of the heavy rain, 16–17 UTC, the latent heat release due to the microphysical processes related to cold cloud decreased significantly. The latent heat releases related to warm cloud processes varied relatively little,

which demonstrates that the weakening of cold cloud processes is greatly related to the decaying of heavy rain. There was little difference in total latent heat release among the three time periods. However, there was a difference in the releases of positive and negative latent heats. With the development of heavy rain, the releases of positive and negative latent heats differed insignificantly. However, during the decaying stage, they both reduced substantially, but the degree of reduction was similar between the two. Therefore, the variation in the total latent heat was small; however, the negative latent heat was far smaller than the positive latent heat in terms of reduction rate.

Table 2. Latent heat releases of different time periods in different cloud microphysical processes (unit: 10^{14}Jh^{-1}).

WDM6	Physical meaning	14 UTC-15 UTC		15 UTC-16 UTC		16 UTC-17 UTC	
		release	pct.	release	pct.	release	pct.
cond	Water vapor condenses into cloud water	**88.71**	**51.63%**	**95.70**	**54.33%**	**94.10**	**65.69%**
idep	Cloud ice deposition growth	15.66	9.11%	15.41	8.75%	11.69	8.16%
sdep	Snow deposition growth	12.28	7.15%	11.24	6.38%	2.80	1.95%
igen	Initialization of cloud ice	4.04	2.35%	4.03	2.29%	0.80	0.56%
gdep	Graupel deposition growth	16.50	9.60%	14.29	8.11%	4.05	2.83%
aacw	Cloud water collected by snow and graupel	3.30	1.92%	3.17	1.80%	1.35	0.94%
rcond	Water vapor condenses into rainwater	**24.48**	**14.25%**	**23.95**	**13.60%**	**23.61**	**16.48%**
Iacr	Rainwater collected by cloud ice	0.98	0.57%	0.91	0.52%	0.83	0.58%
Gacr	Rainwater collected by graupel	4.87	2.83%	6.11	3.47%	3.48	2.43%
Sacr	Rainwater collected by snow	0.68	0.40%	0.77	0.44%	0.51	0.36%
Ihmf	Homogeneous growth of cloud ice	0.00	0.00%	0.00	0.00%	0.00	0.00%
Gfrz	Rainwater condenses into graupel	0.11	0.06%	0.20	0.11%	0.00	0.00%
Ihtf	Heterogeneous growth of cloud ice	0.19	0.11%	0.37	0.21%	0.00	0.00%
Cact	Activation of cloud condensation nuclei	0.00	0.00%	0.00	0.00%	0.00	0.00%
Cevp	Evaporation of cloud water into water vapor	-1.56	4.33%	-1.21	2.65%	-0.85	8.92%
Revp	Evaporation of cloud water into water vapor	**-13.55**	**37.62%**	**-21.64**	**47.35%**	**-3.20**	**33.58%**
Ssub	Sublimation of snow	-1.75	4.86%	-2.37	5.19%	-1.42	14.90%
Gmlt	Melting of graupel	**-10.14**	**28.15%**	**-9.37**	**20.50%**	**-2.20**	**23.08%**
Isub	Sublimation of cloud ice	-0.24	0.67%	-0.77	1.68%	-1.29	13.54%
Gsub	Sublimation of graupel	-0.55	1.53%	-0.52	1.14%	-0.16	1.68%
Geml	Enhanced melting of graupel	-6.03	16.74%	-7.76	16.98%	-0.36	3.78%
Smlt	Melting of snow	-0.13	0.36%	-0.05	0.11%	-0.02	0.21%
Gevp	Evaporation of melting graupel	-1.98	5.50%	-1.95	4.27%	-0.03	0.31%
Sevp	Evaporation of melting snow	-0.04	0.11%	-0.02	0.04%	0.00	0.00%
Seml	Enhanced melting of snow	-0.07	0.19%	-0.05	0.11%	-0.01	0.10%
Imlt	Melting of cloud ice	0.00	0.00%	0.00	0.00%	0.00	0.00%
The total positive latent heat		171.81		176.14		143.24	
The total negative latent heat		-36.02		-45.70		-9.53	
The total latent heat		135.79		130.44		133.71	

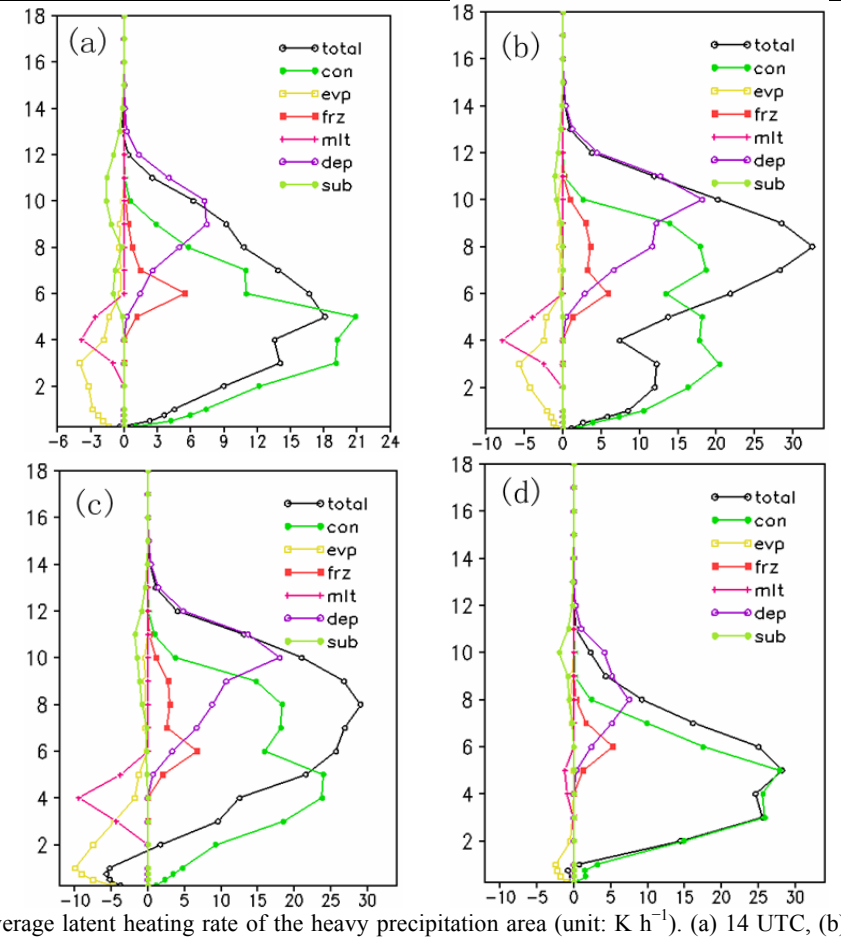

Figure 3. Regional average latent heating rate of the heavy precipitation area (unit: K h^{-1}). (a) 14 UTC, (b) 15 UTC, (c) 16 UTC, and (d) 17 UTC.

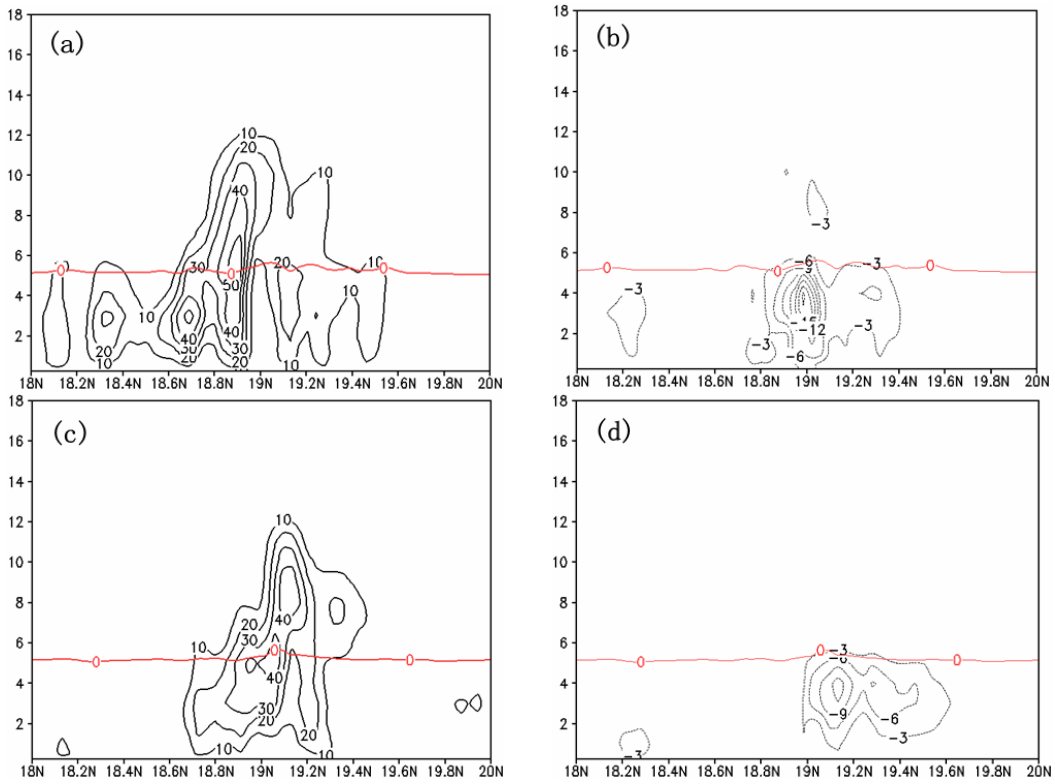

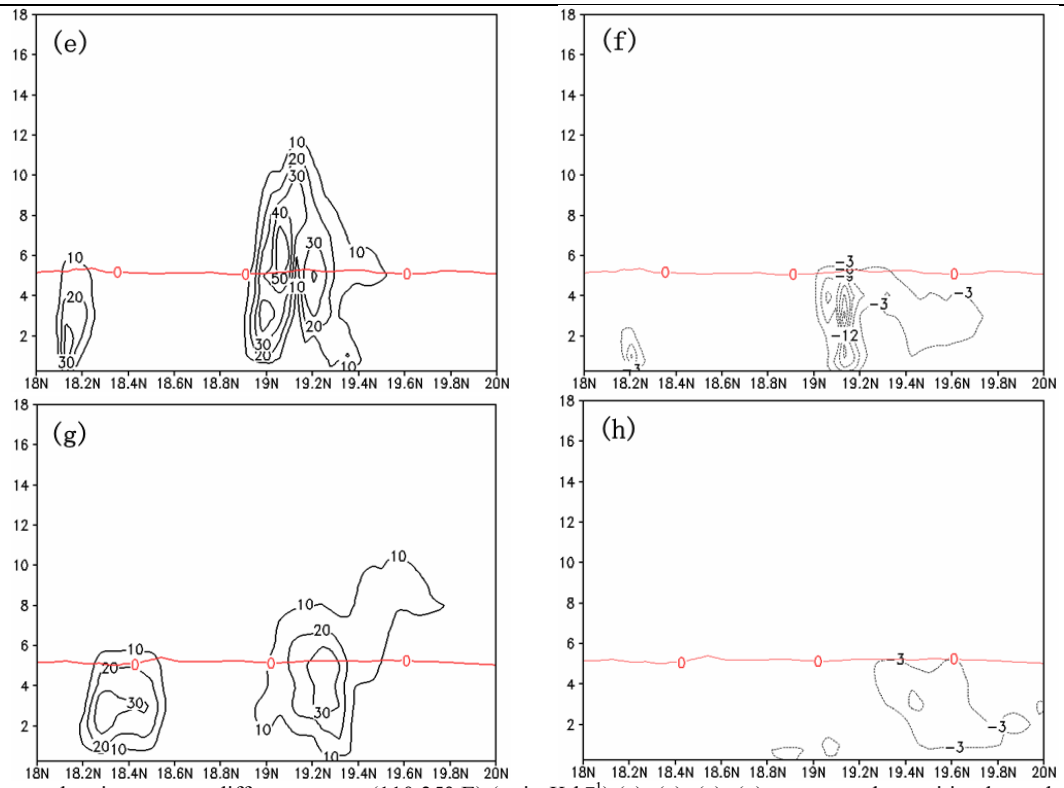

Figure 4. Latent heating rates at different stages (110.35° E) (unit: K h^{-1}).(a), (c), (e), (g) represent the positive latent heating at 14, 15, 16, and 17 UTC, respectively, and (b), (d), (f), (h) represent the negative latent heating at 14, 15, 16, and 17 UTC, respectively.

6 IMPACT OF THE LATENT HEAT OF CLOUD MICROPHYSICAL PROCESSES ON HEAVY RAIN

To discuss the impact of the latent heat due to different cloud microphysical processes on the heavy rain event, a sensitivity test was performed in which the latent heat release of different resources was altered based on the WDM6 cloud microphysical scheme (Table 3). The simulated time was from 00 UTC 5 October 2010 to 00 UTC 6 October 2010. The first 6 hours were simulated using the original WDM6 cloud microphysical scheme. The remaining 18 hours were simulated using the altered scheme.

Compared with CNTL, the other three sensitivity tests showed a weakening of the total precipitation at different scales (Fig.5). The reduction was largest in NREVP, followed by NLS. The precipitation simulated in NLF was slightly smaller than that simulated in CNTL.

The vertical temporal height profiles were made at 110.35° E,19.16° N, a point located within the heavy rain center area (Fig.6), starting from 06 UTC. From 09 UTC, the vertical rising velocity in the high levels strengthened in CNTL. With the strengthening of the vertical motion in the high levels, the air in the low levels changed from descending into ascending, providing favorable conditions for the development of precipitation. In response, the rainfall amount increased. The comparison of the several strengthening processes of precipitation in CNTL shows that during all these processes of the heavy rain event, the vertical rising motion strengthened at high levels, leading to the strengthening of the vertical motion at low levels. Therefore, the precipitation increased rapidly. In NLS, the heating due to deposition was eliminated in the high levels. The results show that the vertical rising motion in high levels did not enhance at 09 UTC and therefore the precipitation did not enhance as rapidly as in CNTL. In experiment NLF, the melting and cooling in middle levels was eliminated, and the vertical velocity increased at a smaller extent than in CNTL. With the strengthening of the rising air in high levels, the air in low levels began to rise rapidly, which enhanced the precipitation at a later time than in CNTL. During the heavy rain event, there was a major contribution of latent heat due to the condensation of rainwater to the total positive latent heat. Without this process, the total latent heating of the atmosphere and thus the convection would weaken dramatically. Therefore, in NREVP, the vertical velocity substantially decreased rather than increased, which is not a favorable condition for precipitation.

As seen from the total latent heating rate (Fig.7), in CNTL, the latent heat release was mainly positive after 06 UTC. The heating effect was strong from around 12 km to the surface and the strong heating center was located at 8 km. In NLS, the heating above

8 km weakened substantially and large areas of negative latent heating occurred. The heating center was located at around 4 km. The distribution of positive latent heat was located higher in NLF than in CNTL. Negative latent heating area occurred above 10 km; however, the heating increased below 6 km. Compared with in CNTL, the total latent heating decreased greatly in NREVP.

Table 3. Design of the sensitivity test.

Experiment	Description
CNTL	WDM6 cloud microphysical scheme
NLS	WDM6 cloud microphysical scheme without the latent heat release due to deposition and sublimation
NLF	WDM6 cloud microphysical scheme without the latent heat release due to congelation and melting
NREVP	WDM6 cloud microphysical scheme without the latent heat release due to the condensation of rainwater and evaporation

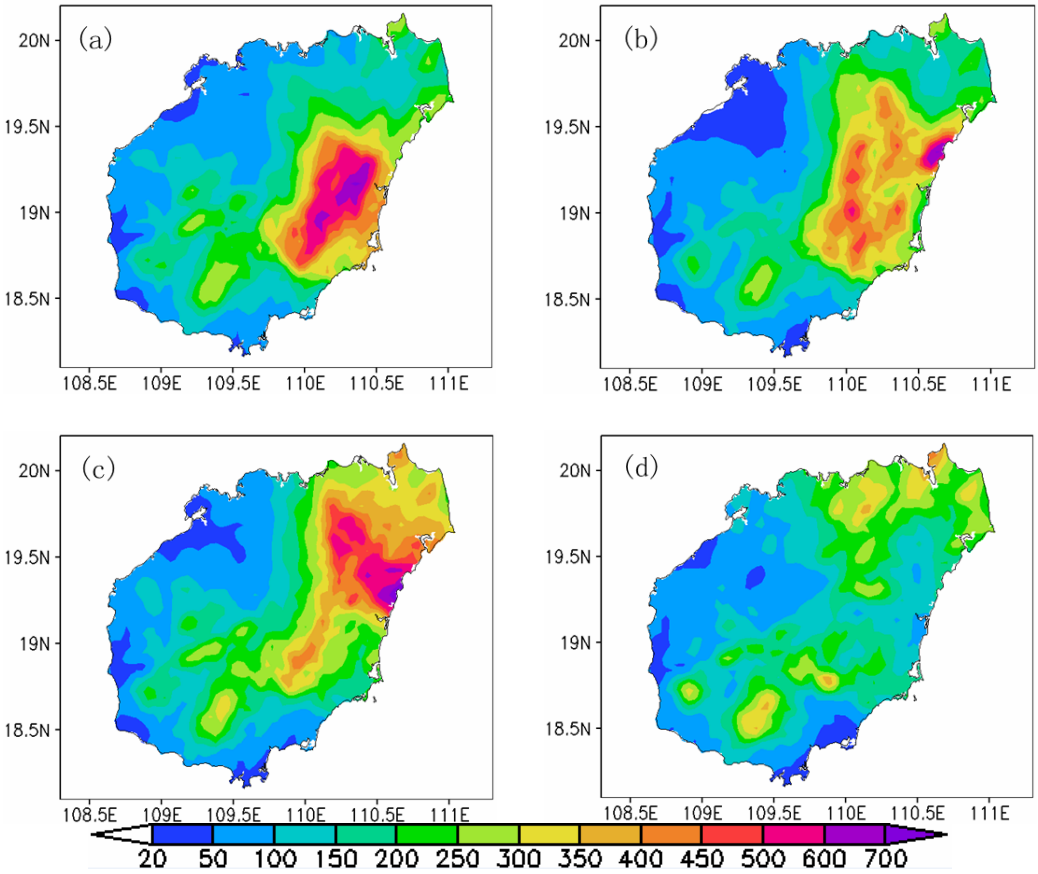

Figure 5. The 24-hour accumulated precipitation of different simulation experiments. (a) CNTL, (b) NLS, (c) NLF, and (d) NREVP.

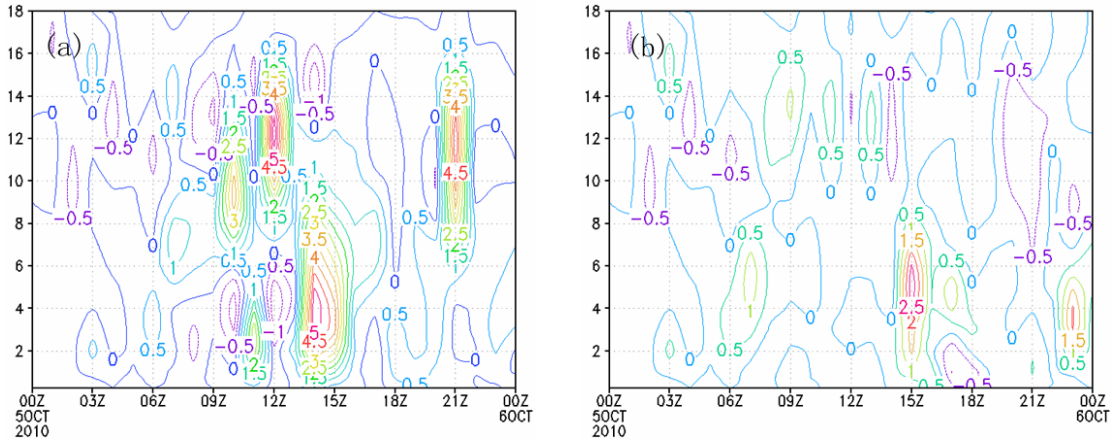

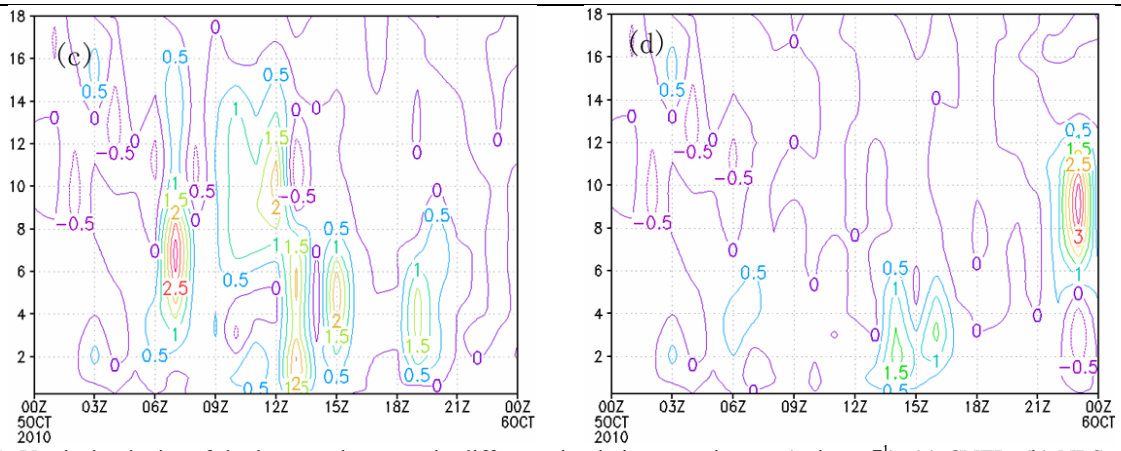

Figure 6. Vertical velocity of the heavy rain center in different simulation experiments (unit: ms^{-1}). (a) CNTL, (b) NLS, (c) NLF, and (d) NREVP.

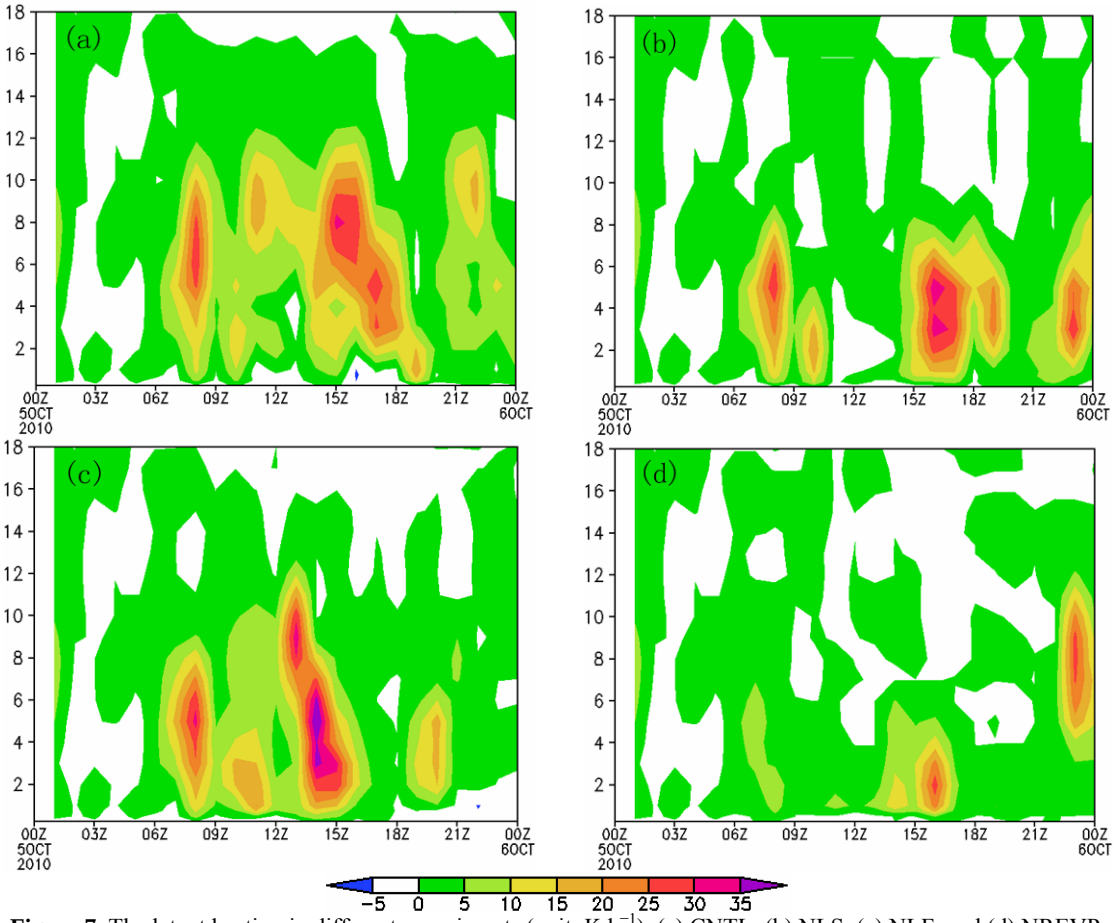

Figure 7. The latent heating in different experiments (unit: K h^{-1}). (a) CNTL, (b) NLS, (c) NLF, and (d) NREVP.

7 CONCLUSIONS

In this paper, we analyzed the heavy rain process over Hainan Island from 5 October 2010 to 6 October 2010 through simulation using the mesoscale numerical model WRF and WRF-3DVAR system. The analysis focused on the cloud microphysical latent heat characteristics of the heavy rain development process. Sensitivity tests were also used to investigate the impact of different cloud microphysical latent heat processes on the heavy rain simulation. The results are as follows:

The heating center of the total latent heat was located above the melting layer. The heating was intensive and reached 8 km. With the weakening of the rising air, descending air appeared at low levels. When the heavy rain was decaying, all moisture variables decreased significantly. The latent heating at high levels also weakened significantly. The heating center was located below the melting layer. During the strengthening process of the heavy rain event, the

precipitation mainly resulted from the melting and enhanced melting of graupel. During the decaying processes of the heavy rain event, the precipitation mainly resulted from the conversion of cloud water into rainwater.

During the heavy rain event, the positive latent heat was distributed above 12 km, far above the melting layer. The maximum heating center was at 6–8 km and the negative latent heating was mainly located below the melting layer. Its maximum was at 4 km. The positive latent heat was far stronger than the negative latent heat and mainly resulted from the condensation process. The latent heats of deposition, congelation, melting and evaporation all weakened after initially strengthening during the heavy rain event. There was little variation in the latent heats of condensation and sublimation. During the decaying stage, the positive and negative latent heats both decreased; however, the negative latent heat decreased to a larger extent. The main cloud microphysical processes of the positive latent heat release were condensation of water vapor into cloud water, the condensation of rainwater, and the deposition growth of cloud ice, snow and graupel. The main cloud microphysical processes of the negative latent heat release were the evaporation of rainwater, the melting and the enhanced melting of graupel.

The latent heat release due to different cloud microphysical processes have a major impact on the precipitation intensity. Without the condensation and evaporation of rainwater, the total latent heating will weaken and the moisture variables and the precipitation will substantially decrease. Without the deposition and sublimation processes, the heating at high levels and the precipitation will weaken; however, the extent of this weakening will not be as substantial as that for the exclusion of condensation and evaporation of rainwater. Without the congelation and melting processes, the latent heating at low levels will enhance. The distribution of moisture variables will not change substantially but the precipitation will decrease considerably.

REFERENCES:

[1] MENG Wei-guang, WANG An-yu, LI Jiang-nan, et al. Numerical simulation of a Mesoscale convective system (MCS) during first rainy season over south China [J]. Acta. Meteorol Sinica, 2003, 17(1): 79-92 (in Chinese).

[2] MENG Wei-guang, LI Jiang-nan, WANG An-yu, et al. Effects of condensation heating and surface fluxes on the development of a south china mesoscale convective system (MCS) [J]. J Trop Meteorol, 2005, 11(2): 144-153.

[3] LIN Wen-shi, WU Jian-bin, LI Jiang-nan, et al. An sensitivity simulation about cloud microphysical processes of typhoon Chanchu [J]. J Trop Meteorol, 2010, 16(4): 390-401

[4] LIN W S, XU S S, SUI C H. A numerical simulation of the effect of the number concentration of cloud droplets on Typhoon Chanchu [J]. Meteorol Atmos Phys, 2011, 113(3-4): 99-108

[5] LI J N, WANG G, LIN W S, et al. Cloud-scale simulation study of Typhoon Hagupit (2008) Part I: Microphysical processes of the inner core and three-dimensional structure of the latent heat budget [J]. Atmos Res, 2013, 120: 170-180.

[6] LI J N, WANG G, LIN W S, et al. Cloud-scale simulation study of Typhoon Hagupit (2008) Part II: Impact of cloud microphysical latent heat processes on typhoon intensity [J]. Atmos Res, 2013, 120: 202-215.

[7] WANG Peng-yu, ZHENG Ruan. Mesoscale numerical forecast for supercooled cloud water in convective cloud of South China—— The main meteorological factor responsible for aircraft icing [J]. J Trop Meteorol, 2002, 18(4): 399-406 (in Chinese).

[8] WANG Peng-yu, ZHENG Rong, KANG Hong-wen. Numerical study on cloud physical processes of heavy rainfall in South China [J]. J Appl Meteorol Sci, 2002, 13(1): 78-87 (in Chinese).

[9] FOVELL R G, OGURA Y. Numerical simulation of a midlatitude squall line in dimensions [J]. J Atmos Sci, 1998, 45:3846-3879.

[10] TAO W K, SIMPSON J. Modeling study of a tropical squall-type convective line [J]. J Atmos Sci, 1989, 46(2): 177-202.

[11] COLLE, ZENG Y. Bulk microphysical sensitivities within the MM5 for orographic precipitation. Part I: The Sierra 1986 event [J]. Mon Wea Rev, 2004, 132: 2 780-2 801.

[12] ZHANG C H. Analysis of the non-tropical cyclone rainstorm in the condition of reciprocity between the middle latitude cold air and the low latitude warm low in Hainan Island [J]. J Guangxi Meteorol, 2003, 24(4): 19-21 (in Chinese).

[13] WU Chun-wa, ZHAO Fu-zhu, LI Xun. Analysis of an autumn rainstorm in Hainan Island [J]. Meteorol Disas Reduct Res, 2010, 33(3): 42-48 (in Chinese).

[14] MA Xue-kuan, FU Jiao-lan, CAO Dian-bin. Study on physical mechanism of the persistent heavy rainfall event in autumn 2008 over Hainan [J]. Meteorol Mon, 2012, 38(7): 795-803 (in Chinese).

[15] ZHAO Fu-zhu. Preliminary study on circulation characteristics and mechanism of rainstorm in autumn of Hainan Island [J]. Chin J Trop Agricult, 2011, 31(5): 50-57 (in Chinese).

Citation: LI Jiang-nan, MAI Xue-hu, LI Fang-zhou et al. Characteristics of the latent heat due to different cloud microphysical processes and their influence on an autumn heavy rain event over Hainan Island [J]. J Trop Meteorol, 2016, 22(S1): 57-66.